Journal of Nuclear Materials 406 (2010) 285–292

Contents lists available at ScienceDirect

Journal of Nuclear Materials

journal homepage: www.elsevier.com/locate/jnucmat

Uranium adsorption studies on aminopropyl modified mesoporous sorbent (NH_2–MCM-41) using statistical design method

Şenol Sert *, Meral Eral

Ege University, Institute of Nuclear Sciences, 35100 Bornova-Izmir, Turkey

ARTICLE INFO

Article history:
Received 19 March 2010
Accepted 23 August 2010

ABSTRACT

MCM-41 has been synthesized and modified in order to graft amine groups on its surface. The modified NH_2–MCM-41 adsorbent was characterized by using XRD, SEM, surface area and porosity analyzer, and FT-IR. This characterized adsorbent was investigated for uranium adsorption using the batch method. The central composite design (CCD) combined with the response surface methodology (RSM) was selected to determine the effects of parameters and their interactions for the removal of UO_2^{2+} ions. The optimum values of the parameters determined were 4.2 for the initial pH, 60 °C for the temperature, 90 mg L^{-1} for the initial concentration and 173 min for the shaking time using the response surface methodology. ΔH° and ΔS° were calculated from the slope and the intercept of plots of ln K_d versus $1/T$. The isotherm models, Langmuir, Freundlich, Dubinin–Radushkevich (D–R) have been studied to explain the adsorption characteristics.

1. Introduction

Uranium is likely to occur as a contaminant in the environment as a result of emissions from the nuclear industry, releases in mill tailings, the combustion of coal and other fuels, the use of phosphate fertilizers that contain uranium, machining of depleted-U munitions and natural weathering of igneous rocks and ore bodies which can produce groundwater seeps in the hundreds to thousands of l μg L^{-1} (ppb) range of dissolved uranium [1]. The permissible discharge level of uranium for nuclear industries ranges from 0.1 to 0.5 mg L^{-1}. As per the standards of World Health Organization, the U(VI) concentration in water should not exceed 0.05 mg L^{-1} [2].

The use of conventional treatment methods such as chemical precipitation, reverse osmosis, ion-exchange, filtration, and evaporative recovery are most effective for the treatment of liquid effluents containing high concentration of metal ions. However these technologies become expensive or inefficient for the treatment of effluents containing metal ions in the range of 100 mg L^{-1} [3].

Adsorption is one of the important techniques in separation and purification processes. Adsorption of uranium onto various solids is important from the purification, environmental and radioactive waste disposal points of view [4]. The adsorption of uranium has been the subject of several investigations; activated carbon [5], natural zeolite [6], kaolinite [7], bentonite [8] and montmorillonite [9], alginate [10], iron oxides species; goethite [11] and akaganeite [12] were used as adsorbents for uranium.

Mesoporous molecular sieve materials, known as M41S, were discovered by Kresge et al. and Beck et al. in 1992 [13,14]. In the M41S family, the main structures are hexagonal phase MCM-41; cubic phase MCM-48; and MCM-50, a non stable lamellar phase [15]. MCM-41, which stands for Mobil Composition of Matter No. 41, shows a highly ordered hexagonal array of uni-dimensional pores with a very narrow pore size distribution [16]. The striking features of MCM-41 such as having a very large BET surface area, large pore volume and fast kinetics of sorption attracted many researchers to utilize it as a sorbent and study its sorption behavior towards chemical and radio-toxic metal ions from various waste streams. Stamberg et al. investigated sorption of uranium on MCM-41 as a function of pH, time, U(VI) and CO_3^{-2} concentrations [17]. Salicylaldehyde functionalized mesoporous silica (MCM-41) was utilized for the separation, pre-concentration and determination of uranium in natural waters [18]. The spherical mesoporous silica (MCM-41) is investigated for the recovery of uranium ions from sea water by Lee et al. [19]. Carbamoylphosphonate silane was used for the modification of MCM-41 for sequestration of actinides [20,21]. Lanthanide separations were studied by Gly-UR., Ac-Phos., and Prop-Phos. silane modified MCM-41 [22].

The adsorption of pollutant metal ions by functionalized mesoporous silicas containing amino or thiol groups has been previously investigated. MCM-41 grafted with aminopropyl (NH_2–MCM-41), functionalized with tris-(methoxy) mercaptopropylsilane, amino-functionalized with Fe^{3+} coordination, and modified with thiol were used for $Cr_2O_7^{-2}$ [23], mercury [24], oxyanions [25], and Hg^{+2} [26], respectively.

In this work, aminopropyl modified MCM-41 (NH_2–MCM-41) is prepared for the adsorptions of UO_2^{2+} from aqueous solutions. The

* Corresponding author.
E-mail address: senol.sert@ege.edu.tr (Ş. Sert).

0022-3115/$ - see front matter © 2010 Elsevier B.V. All rights reserved.
doi:10.1016/j.jnucmat.2010.08.024

effects of initial pH, shaking time, initial concentration and temperature on the sorption are discussed using experimental design methodology. Experimental design aims at limiting the number of experiments normally required to study the influence of the most important factors involved in a give reaction [27]. In order to identify the adsorption process, the adsorption data are fitted by Langmuir, Freundlich and D–R isotherm models and the thermodynamic parameters such as ΔH°, ΔS° and ΔG° are calculated.

2. Materials and methods

Mesoporous molecular sieve, MCM-41 preparation and aminopropyl modification were adapted from the previously reported methods [18,28,30]. The reactants for the synthesis of mesoporous molecular sieves at room temperature were tetraethylorthosilicate (TEOS, 99%, Merck), distilled water, hexadecyltrimethylammonium bromide (CTABr, 99%, Merck). Ammonium hydroxide (NH_4OH, 25% Merck) was used as a base source. The MCM-41 was crystallized from the alkaline synthesis solution with a molar composition of 525(H_2O)/69(NH_4OH)/0.125(CTABr)1(TEOS). The detailed preparation procedure can be described as follows: 205 mL of NH_4OH (25 wt.% solution) were mixed with 270 mL of distilled water; 2.0 g of surfactant were added into the solution with stirring until the solution became homogenous. 10 mL of TEOS were introduced, giving rise to a white precipitation. After 2 h, the resulting product was filtered, washed with distilled water, and dried at 50 °C followed by calcinations in air at 823 K for 4 h at a heating rate of 1 °C min^{-1} [28].

The MCM-41 material is modified by nitrogen donor atoms that are expected to favor the binding and the adsorption of uranyl ions from aqueous medium [29]. Modification of the prepared MCM-41 was performed as follows: 2 g of MCM-41 was suspended in 70 mL of dry toluene (99%, Merck) and then 1 g of 3-aminopropyl trimethoxysilane (AMPS, 99%, Merck) was added under dry nitrogen atmosphere and the mixture was refluxed for 12 h. The resulting adsorbent was recovered by filtration, washed with acetone then water, and dried under vacuum [18,30].

Uranium stock solutions (1 g L^{-1}) were prepared from $UO_2(NO_3)_2{\cdot}6H_2O$ (Merck) in deionized water. The working solutions were prepared by diluting the stock solutions to appropriate volumes. The pH values of these solutions were adjusted with 1 mol L^{-1} Na_2CO_3 and 1 mol L^{-1} HNO_3 solution by using Metrohm 654 pH meter with a combined pH electrode. Ultrapure water (resistivity 18.2 MW cm, TOC level 1–5 ppb) was prepared by the Milli-Q (Millipore, Milford, MA, USA) water purification system.

2.1. Characterization of materials

Several instrumental techniques were used for sample characterization. Scanning electron microscope (SEM) images were taken using Phillips XL-30S FEG scanning electron microscope. The SEM image (Fig. 1) showed that MCM-41 particles had similar morphology; hexagonal or the ellipsoid shape originating from hexagonal analogs in the 500–1000 nm scale.

Powder X-ray diffraction (XRD) data were collected using Phillips X'Pert Pro diffractometer with Cu Kα radiation. The data were collected at room temperature in the range of 1.75–7.00 Å. Fig. 2 shows a sample which displays all the characteristic X-ray diffraction peaks of MCM-41 [16]. The XRD pattern of MCM-41 showed three diffraction peaks that can be indexed to (1 1 0), (1 1 0) and (2 0 0). A strong diffraction peak in the low angle region is associated with the (1 0 0) reflection. Two additional weak peaks indexed to the (1 1 0) and (2 0 0) reflections of the typical hexagonal cell are observed.

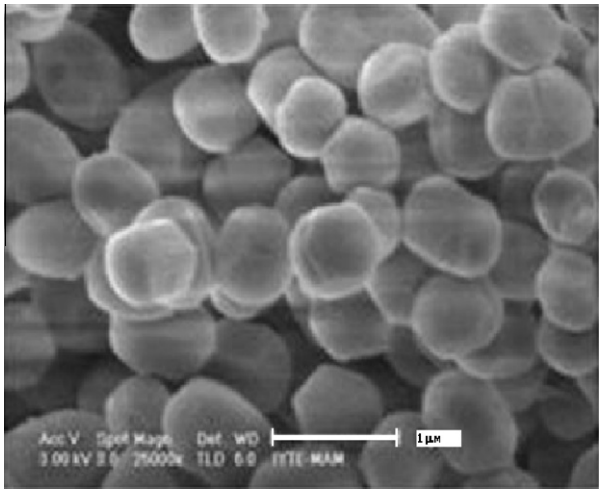

Fig. 1. A scanning electron microscopy picture of MCM-41.

Surface area and porosity were determined from the nitrogen adsorption–desorption isotherms obtained on a Micromeritics ASAP 2020 analyzer. The nitrogen adsorption–desorption isotherms (Fig. 3) of both unmodified and amine-modified samples can be considered as being type IV. The specific (BET) surface area, the pore diameter and the total pore volume are found from the corresponding nitrogen sorption isotherms and summarized in Table 1. It can be seen in Table 1 that grafting of organic functional moieties on MCM-41 results in the decrease of the specific surface area and pore size. The surface area decreased by 40% after the grafting of $C_3H_6NH_2$ groups on MCM-41. The pore size of NH_2–MCM-41 (1.9 nm) is smaller than that of MCM-41 (2.9 nm) due to the alkyl chain.

Fourier transform infrared spectroscopy (FT-IR) was performed by the Shimadzu FT-IR-8400S spectrometer using the KBr pellet method. The FT-IR spectra of MCM-41 and NH_2–MCM-41 are shown in Fig. 4. The broad absorption band in the region 3765–3055 cm^{-1} can be attributed to the stretching of the framework Si–OH group with defective sites and physically adsorbed water molecules. The vibrations of Si–O–Si can be seen at 1095 cm^{-1} (asymmetric stretching), 814 cm^{-1}(symmetric stretching) and 460 cm^{-1} (bending) [31]. Typical (C–H) stretching vibrations of the propyl chains at ca. 2900 cm^{-1} together with (NH_2) bending bands at 1570 cm^{-1} confirmed the grafting of amino propyl groups in all functionalized samples [32].

2.2. Batch adsorption experiments

Batch adsorption experiments were performed by a thermostatically controlled shaker (GFL-1083 model). In the experiments, 0.005 g NH_2–MCM-41 adsorbent was shaken with 30 mL UO_2^{2+} solutions at varying experimental conditions in 50 mL Erlenmeyer flasks at a speed of 150 rpm.

The supernatants were filtered through a filter paper (Whatman No. 41) and the concentration of UO_2^{2+} in the solution was measured by a Perkin–Elmer Optima 2000 DV ICP-OES before and after the establishment of equilibrium. The amount of UO_2^{2+} ions adsorbed by NH_2–MCM-41 was calculated using the following equation:

$$Q = (C_o - C_e) \times \frac{V}{m}, \quad (1)$$

where Q is the metal uptake (mg g^{-1}), C_o and C_e are the initial and equilibrium UO_2^{2+} concentrations in the solution (mg L^{-1}), respectively, V is the solution volume (L) and m is the mass of sorbent

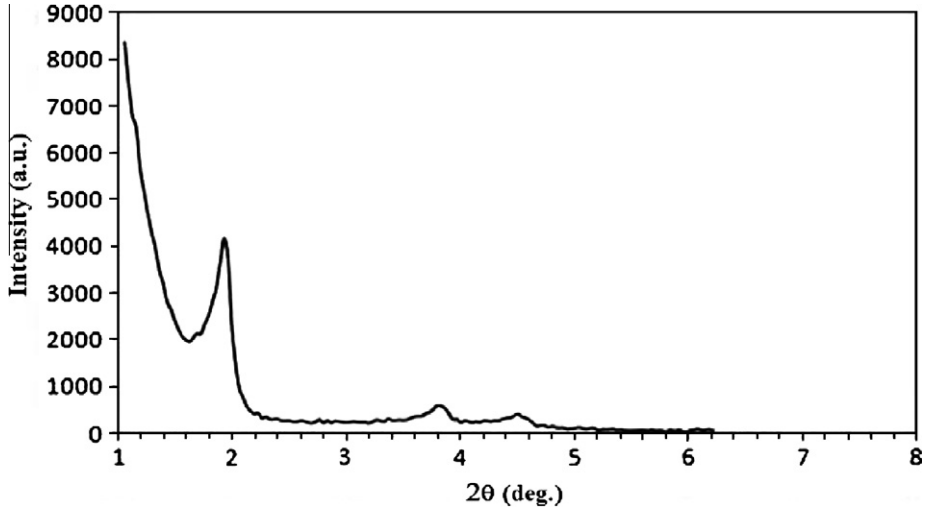

Fig. 2. X-ray diffractions of MCM-41.

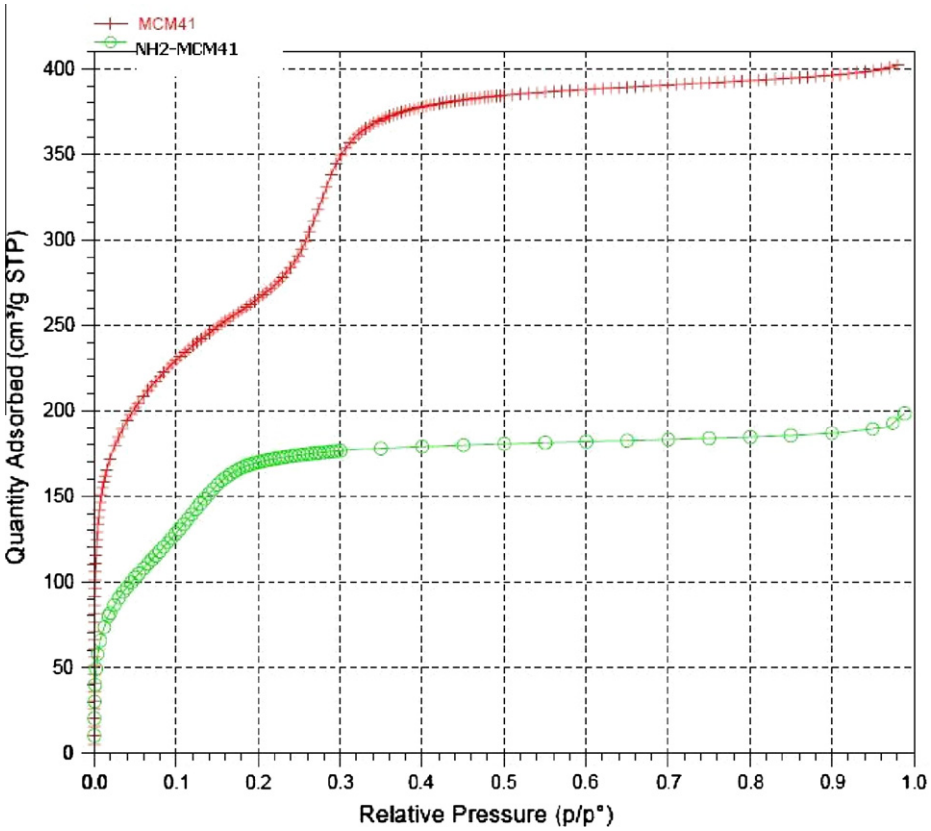

Fig. 3. Adsorption isotherm of nitrogen on MCM-41 and NH_2–MCM-41.

Table 1
Physical and chemical properties of the prepared adsorbents.

	Surface functional group	BET surface area ($m^2\ g^{-1}$)	BJH adsorption average pore diameter (nm)
MCM-41	–OH	956	2.9
NH_2–MCM-41	$-CH_2CH_2CH_2NH_2$	577	1.9

(g). The distribution coefficient K_d ($mg\ L^{-1}$) of metal ions between the aqueous phase and the solid phase can be directly obtained using:

$$K_d = \frac{C_o - C_e}{C_e} \times \frac{V}{m}, \tag{2}$$

where C_o ($g\ L^{-1}$) and C_e ($g\ L^{-1}$) are the initial and equilibrium UO_2^{2+} concentrations, respectively, V/m is the ratio of the volume of metal solution (mL) to the amount of adsorbent (g) in a batch.

2.3. Experimental design for adsorption studies

The optimum condition for sorption of UO_2^{2+} ions by NH_2–MCM-41 was determined by means of the central composite design

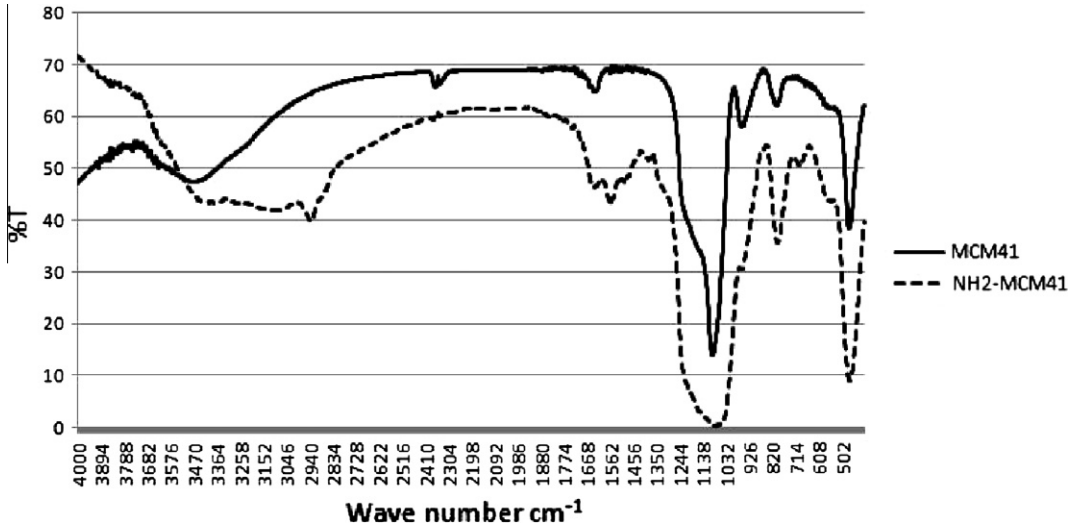

Fig. 4. FT-IR spectra of MCM-41 and NH_2–MCM-41.

(CCD) under response surface methodology (RSM). Statistical design of experiments refers to the process of planning to experiments so that appropriate data that can be analyzed by statistical methods will be collected resulting in valid and objective conclusions [33]. Response surface methodology is a collection of mathematical and statistical techniques based on the fit of a polynomial equation to the experimental data, which must describe the behavior of a data set with the objective of making statistical previsions [34].

The experiments were carried out by the four independent process variables, initial pH (X_1), temperature (X_2), initial UO_2^{2+} concentration (X_3) and shaking time (X_4) chosen according to the central composite design (CCD). The optimization of UO_2^{2+} removal was performed using the four chosen independent process variables with seven replicates at centre points, employing a total of 31 experiments in this study. The design matrix for the four variables is varied at five levels ($-\alpha$, -1, 0, +1, $+\alpha$). The full model equation with linear and quadratic terms for predicting the optimal response was given as,

$$y_i = b_0 + \Sigma b_i X_i + \Sigma b_{ii} X_{ii}^2 + \Sigma b_{ij} X_i X_j, \tag{3}$$

In the equation, b_0 represents the intercept. The terms, b_i, b_{ii}, and b_{ij} represent the linear effects, second order effects, and dual interaction between the investigated parameters. For the current model investigated in this study, the second-order polynomial equation can be presented as,

$$\begin{aligned} Y = {} & b_0 + b_1X_1 + b_2X_2 + b_3X_3 + b_4X_4 + b_{11}X_1^2 + b_{22}X_2^2 + b_{33}X_3^2 \\ & + b_{44}X_4^2 + b_{12}X_1X_2 + b_{13}X_1X_3 + b_{14}X_1X_4 + b_{23}X_2X_3 \\ & + b_{24}X_2X_4 + b_{34}X_3X_4. \end{aligned} \tag{4}$$

The range and the level of experimental variables investigated in this study are shown in Table 2.

Table 2
Experimental independent variables.

Factor	Factor code	Levels and range (coded)				
		−2	−1	0	+1	2
Initial pH	X_1	3.5	4.5	5.5	6.5	7.5
Temperature (°C)	X_2	20	30	40	50	60
Initial concentration (mg L^{-1})	X_3	10	30	50	70	90
Shaking time (min)	X_4	15	75	135	195	255

The four variables were varied at two levels (+1 and −1). The higher and the lower levels of the variables were designated as +1 and −1, respectively. The centre point was designated as 0, with −2 and +2 showing star points (α) which are calculated using the following equation:

$$\alpha = [\text{number of factorial points}]^{\frac{1}{4}}. \tag{5}$$

Codification of the variable levels consists of transforming each real value investigated into a coordinate on a scale with dimensionless values proportional to its localization in the experimental space [34].

The following equation can be used to transform a real value (z_i) into a coded value (x_i) for statistical calculations:

$$x_i = \frac{(z_i - z_i^0)}{\Delta z_i}, \tag{6}$$

where Δz_i is the difference between the real values designed for experiments and z^0 the real value at the central point. MatLab 7.1 and Excell were used for regression and graphical analysis of the data obtained. The optimum values of the selected variables were obtained by solving the regression equation and by analyzing the response surface contour plots [33].

3. Result and discussion

3.1. The optimization of adsorption parameters

The effects of experimental variables such as the initial pH, the shaking time, the initial concentration and the temperature on UO_2^{2+} adsorption capacity of the adsorbent were investigated using RSM according to the CCD. The experiments were carried out with 16 factorial points, nine star points (1 at the center) and six replicate points used in the central composite design. The coded experimental data points along with the predicted and observed responses are given in Table 3.

The relationship between the independent variables and the responses are expressed by the following quadratic model:

$$\begin{aligned} Y = {} & 249 - 30.3X_1 + 18.4X_2 + 58.8X_3 + 5.24X_4 - 29.5X_1^2 \\ & - 7.03X_2^2 - 14.0X_3^2 - 17.9X_4^2 - 3.18X_1X_2 - 21.2X_1X_3 \\ & + 3.77X_1X_4 + 14.1X_2X_3 + 7.84X_2X_4 + 3.42X_3X_4. \end{aligned} \tag{7}$$

Table 3
Experimental data points used in CCD statistical design and observed and predicted values for UO_2^{2+} uptake capacity of NH_2–MCM-41.

Run no.	Coded values				Responses (*Y*)	
	X_1	X_2	X_3	X_4	Observed	Predicted
1	1	1	1	1	213.29	237.10
2	1	1	1	−1	172.96	196.54
3	1	1	−1	1	125.13	127.12
4	1	1	−1	−1	107.84	100.25
5	1	−1	1	1	142.12	162.96
6	1	−1	1	−1	142.61	153.76
7	1	−1	−1	1	96.81	109.18
8	1	−1	−1	−1	91.66	113.67
9	−1	1	1	1	356.69	338.99
10	−1	1	1	−1	320.71	313.53
11	−1	1	−1	1	150.03	144.07
12	−1	1	−1	−1	148.81	132.29
13	−1	−1	1	1	239.34	252.13
14	−1	−1	1	−1	255.69	258.03
15	−1	−1	−1	1	132.67	113.41
16	−1	−1	−1	−1	151.60	133.00
17	2	0	0	0	119.64	70.32
18	−2	0	0	0	151.74	191.54
19	0	2	0	0	249.91	257.45
20	0	−2	0	0	201.07	184.01
21	0	0	2	0	340.24	310.19
22	0	0	−2	0	54.64	75.18
23	0	0	0	2	197.33	187.65
24	0	0	0	−2	166.51	166.68
25	0	0	0	0	255.26	248.86
26	0	0	0	0	255.83	248.86
27	0	0	0	0	241.49	248.86
28	0	0	0	0	254.08	248.86
29	0	0	0	0	238.78	248.86
30	0	0	0	0	245.27	248.86
31	0	0	0	0	251.29	248.86

The ANOVA (analysis of variance) of data was carried out at 95% confidence level to check the fitting of the experimental values to the predicted ones (Table 4). *F*-test for the significance level of data gave $P < 0.05$ with a model *F* value of 18.20 revealing that this regression is statistically significant. The correlation coefficient value (R^2) of 94% indicated that there was a high correlation between the observed values and the predicted ones.

Significance of each coefficient present in Eq. (7) is determined by the student's *t*-test and *P*-values [33]. The main effects, main affects squares and the interactions of main affects were statistically analyzed and influences of affects on the adsorption process were considered. The coefficients of independent variables *t* and *P* values according to the investigated parameters are given in Table 5.

The influences of initial pH, temperature and initial concentration on the adsorption process were considered to be statistically significant as main affects ($P < 0.05$). Also the squared values of main affects of initial pH initial concentration and shaking time were considered to be statistically significant.

The interaction affects of initial pH, initial concentration, temperature and initial concentration were considered as significant parameters on the adsorption process.

Table 4
Analysis of variance (ANOVA) for the regression model for UO_2^{2+} uptake capacity of NH_2–MCM-41.

Sources of variation	*df*	Sum of squares	Mean squares	*F*-value	Probability > *F*
Regression	14	159,454	11,390	18.20	<0.0001
Residual	16	10,014	626		
Total	30	169,468			

$R^2 = 0.94$.

Table 5
Estimated regression coefficient and corresponding *t* and *P* values.

Regression	Coefficients	Standard error	*t*	*P*
Intercept	248.8566	9.4556	26.3181	1.339E−14
X_1	−30.3054	5.1066	−5.9344	2.097E−05
X_2	18.3600	5.1066	3.5953	0.0024
X_3	58.7526	5.1066	11.5050	3.778E−09
$X4$	5.2434	5.1066	1.0267	0.3197
X_1X_1	−29.4812	4.6783	−6.3016	1.054E−05
X_2X_2	−7.0311	4.6783	−1.5029	0.1523
X_3X_3	−14.0439	4.6783	−3.0019	0.0084
X_4X_4	−17.9225	4.6783	−3.8309	0.0014
X_1X_2	−3.1800	6.2543	−0.5084	0.6180
X_1X_3	−21.2358	6.2543	−3.3953	0.0036
X_1X_4	3.7727	6.2543	0.6032	0.5548
X_2X_3	14.050	6.2543	2.2464	0.0391
X_2X_4	7.8399	6.2543	1.2535	0.2280
X_3X_4	3.4209	6.2543	0.5469	0.5919

It is known that the larger the coefficient, the larger is the effect of the related parameter. The positive sign also shows that there is a direct relation between the parameter and the dependent variable [35]. When the effect of a factor is positive, an increase in the value of the removal efficiency is observed if the factor changes from low to high level. In contrast, if the effect is negative, a reduction in removal efficiency occurs for the high level of the same factor [36].

The positive values of coefficients related to the initial concentration ($X_3 = 58.75$) and temperature ($X_2 = 18.36$) indicate that the initial concentration and temperature have positive effects on the adsorption. However, initial pH coefficient ($X_1 = -30.30$) has a negative cumulative effect on the adsorption of UO_2^{2+} from aqueous solution by NH_2–MCM-41. However, the observation that the adsorption of UO_2^{2+} increases between pH = 3.5–5 and decreases between pH = 5–7.5 (Fig. 5) should also be taken account when considering the initial pH effect.

The model equation is useful in indicating the direction in which the variables should be changed in order to optimize the uptake capacity of UO_2^{2+}. The optimum experimental values in coded form were found for each parameter for the uptake capacity of UO_2^{2+} by double differentiation:

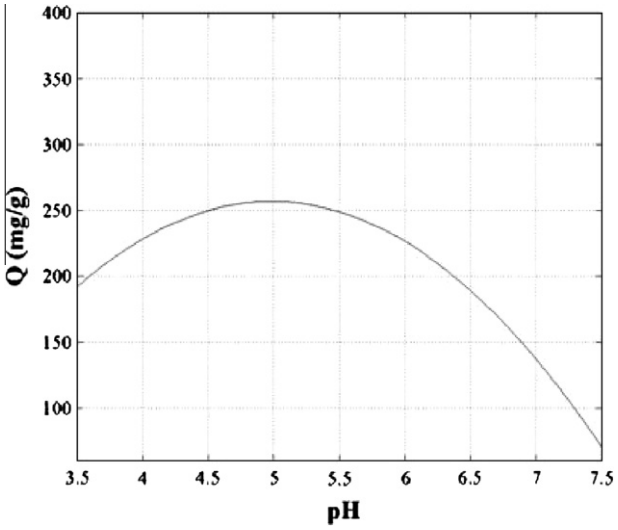

Fig. 5. pH effect on adsorption of UO_2^{2+} from aqueous solution by NH_2–MCM-41 (temperature: 40 °C, concentration: 50 mg L^{-1}, shaking time: 135 min).

$$\frac{dy^2}{dx_1^2} = 0 \quad x_1 = -1.3,$$
$$\frac{dy^2}{dx_2^2} = 0 \quad x_2 = 2,$$
$$\frac{dy^2}{dx_3^2} = 0 \quad x_3 = 2,$$
$$\frac{dy^2}{dx_4^2} = 0 \quad x_4 = 0.63.$$

These coded values can be transformed to real values using Eq. (6). The optimum values giving the maximum uptake of uranium ions (435 mg g^{-1}) were calculated to be at initial pH of 4.2, temperature of 60 °C, initial concentration of 90 mg L^{-1} and shaking time of 173 min.

3.2. Effect of initial pH and initial concentration on the UO_2^{2+} uptake

Effluents from nuclear industry containing uranium have a variable pH (acidic to alkaline) [37]. The effects of initial pH and initial UO_2^{2+} ion concentration on the uptake are shown in Fig. 6. The metal uptake increased with increasing initial solution pH ranging from 3.5 to 5.0; pH values higher than 5.0 reduced the UO_2^{2+} uptake. On the other hand, metal uptake increased with increasing initial metal ion concentration ranging from 10 to 90 mg L^{-1} in all pH ranges.

The increase of metal uptake by increasing initial metal ion concentration is due to an increase in the driving force of the concentration gradient, rather than the increase in the initial metal ion concentration. Under the same conditions, if the concentration of metal ions in the solution is higher, the active sites of adsorbent are surrounded by more metal ions, and the process of adsorption is carried out more effectively. Therefore, the value of Q increased with increasing initial metal ion concentration [38].

At lower pH conditions, UO_2^{2+} uptake was decreased due to increasing positive charge of the adsorbent surface. The NH_2–MCM-41 is completely protonated at pH's less than 2.8 [23]. The metal ions which are expected to be adsorbed are also positively charged, thus the adsorption is not favored. Besides this, H^+ ions present at higher concentrations in the reaction mixture compete with positive ions for the adsorption sites resulting in the further reduction of uranium uptake. On the contrary, as the pH increases, the adsorbent surface becomes more negatively charged and therefore the adsorption of positively charged species is more favorable. As pH is increased from 2.0 to 6.0, the amount of U(VI) adsorbed on NH_2–MCM-41 increased with it [39].

The observed decrease in the uptake of UO_2^{2+} at pH = 5.5 can be explained on the basis of the formation of different uranyl species with lower adsorption affinities. At pH $\geqslant$ 4.8, formations of various oligomeric and monomeric hydrolyzed species of UO_2^{2+} are reported. In the presence of carbonate anions, monomeric and oligomeric carbonate species such as $[UO_2CO_3]^0$, $[UO_2(CO_3)_2]^{2-}$, $[UO_2(CO_3)_3]^{4-}$, and $[(UO_2)_3(CO_3)_6]^{6-}$ may also form at different concentrations depending on the pH and the total concentration of UO_2^{2+} ions [40].

3.3. Effect of initial concentration and temperature on the UO_2^{2+} uptake

The effect of initial concentration and temperature on the uptake of UO_2^{2+} is shown in Fig. 7. The metal uptake increased with increasing temperature ranging from 20 to 60 °C as well as with initial metal ion concentration ranging from 10 to 90 mg L^{-1}. But the adsorption process increases sharply in high temperatures compared to that at low temperatures. This reveals that the temperature affects on adsorption process dramatically.

The increase in uptake starts to decrease around 50 °C under initial concentrations of 60 mg L^{-1}. Initial concentration and temperature combinations are comprised of different maximum adsorption points. This situation can be explained by the establishment of different chemical equilibria between the adsorbent active sites and UO_2^{2+} ions or desorption of UO_2^{2+} ions at high temperature in the given range.

3.4. Determination of thermodynamic parameters

The adsorption processes were carried out 20–60 °C for UO_2^{2+} ions. Adsorption enthalpy was measured using the method based on the van't Hoff plot. The values of $\Delta H°$ and $\Delta S°$ were calculated from the slopes and intercepts of the linear variation of ln K_d, thermodynamic stability constant with reciprocal of temperature $1/T$, (Fig. 8) [41], using the relation:

$$\ln K_d = \frac{\Delta S°}{R} - \frac{\Delta H°}{RT}, \tag{8}$$

where $\Delta H°$ and $\Delta S°$ are the changes in the standard enthalpy (kJ mol^{-1}) and the standard entropy (J mol^{-1} K^{-1}) of adsorption, respectively. T is the absolute temperature (K) and R is the gas constant (8.314 J mol^{-1} K^{-1}). The free energy change, $\Delta G°$, of adsorption is calculated using the equation:

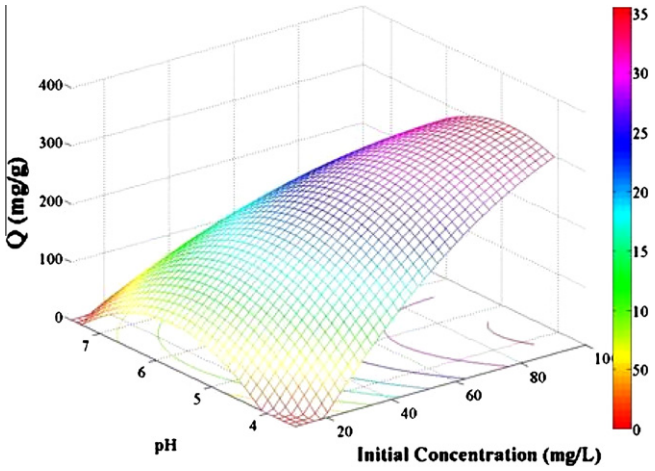

Fig. 6. Response surface plot for the effects of initial concentration and pH on adsorption of UO_2^{2+} from aqueous solution by NH_2–MCM-41.

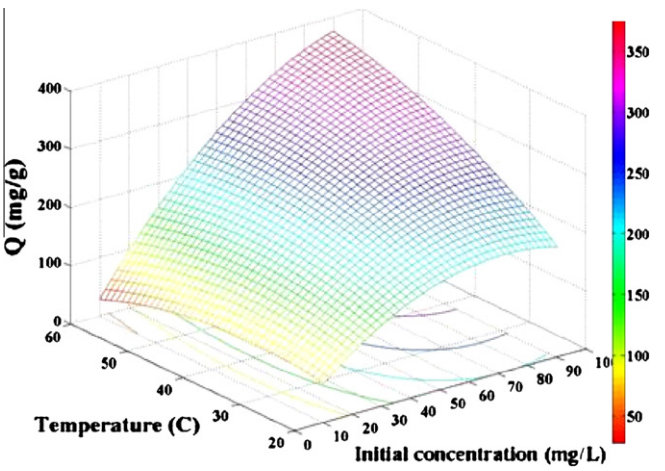

Fig. 7. Response surface plot for the effects of temperature and initial concentration on adsorption of UO_2^{2+} from aqueous solution by NH_2–MCM-41.

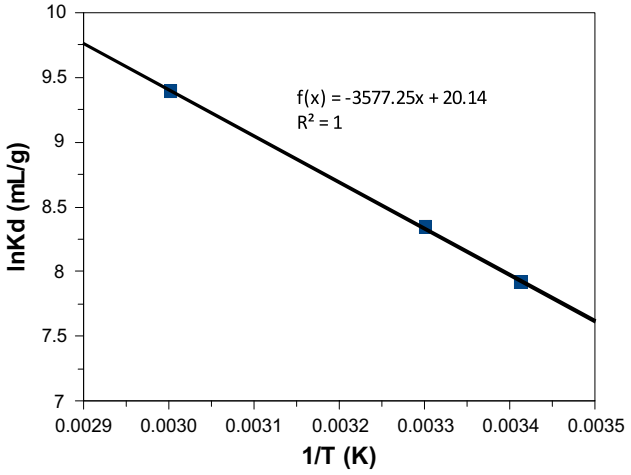

Fig. 8. Plots of ln K_d versus $1/T$ for the UO_2^{2+} adsorption on NH_2–MCM-41 (c: 90 mg L^{-1}, v: 30 mL, pH: 5, t: 15 min, m: 0.01 g).

$$\Delta G^\circ = \Delta H^\circ - T\Delta S^\circ, \tag{9}$$

The values of ΔH°, ΔS° and ΔG° are given in Table 6 for UO_2^{2+} adsorption on NH_2–MCM-41.

The positive value of ΔH° (28.89 kJ mol^{-1}) indicates the endothermic nature of the adsorption process and decrease in the value of ΔG° with rising temperature show that the adsorption is more favorable at high temperatures. In addition, the value of ΔS°(164.12 J mol^{-1} K^{-1}) was found to be positive due to the exchange of metal ions with more mobile ions present on the exchanger which would cause an increase in the entropy during the adsorption process [42].

3.5. Isotherm models

In order to understand the adsorption capacity of the adsorbents, the equilibrium data were evaluated according to the Freundlich, Langmuir and Dubinin–Radushkevich isotherms. These isotherm equations are commonly used for describing adsorption equilibrium for water and wastewater treatment applications [12].

The Langmuir equation, which has been successfully applied to many adsorptions, is given by

$$\frac{C_e}{Q_e} = \frac{1}{bn_m} + \frac{C_e}{n_m}, \tag{10}$$

where C_e is the equilibrium concentration (mg L^{-1}), Q_e is the amount absorbed at equilibrium (mg g^{-1}), n_m and b are the Langmuir constants related to monolayer capacity and energy of adsorption. Langmuir isotherm models the monolayer coverage of the adsorption surface. This model assumes that adsorption occurs at specific homogeneous adsorption sites within the adsorbent and intermolecular forces decrease rapidly with the distance from the adsorption surface. The Langmuir adsorption model is further based on the assumption that all adsorption sites are energetically identical and adsorption occurs on a structurally homogeneous adsorbent [41].

The empirical Freundlich equation, based on sorption on a heterogeneous surface was also applied for the adsorption of UO_2^{2+} [12]:

$$Q_e = KC_e^{1/n}, \tag{11}$$

Eq. (11) can be rearranged to linear form:

$$\log q = \log K + (1/n)\log C_e, \tag{12}$$

where q is the amount of solute adsorbed per unit mass of adsorbent, C_e is the equilibrium concentration, K and n are the Freundlich constants characteristic of a particular adsorption isotherm and can be evaluated from the intercept and slope of the linear plot of log q versus log C_e.

The sorption D–R isotherm model is applicable at low concentration ranges and can be used to describe sorption on both homogeneous and heterogeneous surfaces. This is postulated within an adsorption "space" close to sorbent surface. If the surface is heterogeneous and an approximation to a Langmuir isotherm is chosen as a local isotherm for all sites that are energetically equivalent, then the quantity β (a constant related to energy and Polanyi potential) can be related to the mean sorption energy, ε, which is the free energy of transfer of 1 mol of UO_2^{2+} ions from infinity to the surface of the sorbent [12]. This model can be represented by the general expression:

$$\ln X = \ln X_m - K\varepsilon^2, \tag{13}$$

where ε is Polanyi potential and is equal to,

$$\varepsilon = RT\ln(1 + 1/C_e), \tag{14}$$

X is the amount of metal adsorbed per unit mass of adsorbent, X_m is the theoretical adsorption capacity, C_e is the equilibrium concentration of metal, K is the constant related to adsorption energy, R is the universal gas constant and T is the temperature in Kelvin. From the slopes and intercepts of the linear graphs of ln X and ε^2, the parameters K and X_m were calculated (Table 7). The mean energy of sorption (E) is the free energy change when one mol of ion is transferred to the surface of the solid from infinity in the solution and it is calculated from:

$$E = -(2K)^{-1/2}, \tag{15}$$

The value of E is used to estimate the reaction mechanism occurring. If E is in the range of 8–16 kJ mol^{-1} sorption is governed by ion exchange. In the case of $E < 8$ kJ mol^{-1}, physical forces may affect the sorption mechanism. On the other hand, if $E > 16$ kJ mol^{-1} sorption may be dominated by particle diffusion:

The corresponding Freundlich, Langmuir and D–R parameters along with their correlation coefficients are reported in Table 7.

Based on the value of the correlation coefficient ($R^2 = 0.99$) it can be seen that the behavior of UO_2^{2+} adsorption onto NH_2–MCM-41 is a Langmuir type isotherm. The calculated E value

Table 6
Thermodynamic parameters for the UO_2^{2+} adsorption on the NH_2–MCM-41.

ΔH° (kJ mol^{-1})	ΔS° (J mol^{-1} K^{-1})	ΔG° (kJ mol^{-1})		
		293 K	303 K	333 K
29.74	167.00	−19.32	−20.99	−26.02

Table 7
Langmuir, Freundlich and D–R constants for the adsorption of UO_2^{2+} on NH_2–MCM-41.

Adsorbent	Langmuir model			Freundlich model				D–R model		
NH_2–MCM-41	R^2	n_m (mg g^{-1})	b (L mg^{-1})	R^2	K (mg g^{-1})	n	R^2	X_m (mmol g^{-1})	E (kJ mol^{-1})	K
	0.995	625	0.106	0.9239	86.19	2.21	0.9542	0.0105	12.31	0.003

for UO_2^{2+} adsorption is 12.31 kJ mol^{-1}. This value is in the range of 8–16 kJ mol^{-1}, so sorption is governed by ion exchange for adsorbent.

4. Conclusion

In this work, MCM-41 has been synthesized with very high surface area and is modified in order to graft amine groups on the surface. The uranium uptake experiments have been carried out by the batch method. The affecting parameters were analyzed by using central composite design as the experimental design method. Variance analysis of data was carried out at 95% confidence level and the fitting of experimental values to predicted ones was checked using ANOVA. The *F*-test gave $P < 0.05$ with a model *F* value of 18.20 which revealed that this regression is statistically significant. The correlation coefficient value (R^2) of 94% indicated that there was a high correlation between the observed values and the predicted ones.

The initial concentration and temperature have positive effects on the adsorption. The adsorption of UO_2^{2+} increases at pH = 3.5–5.5 and decreases at pH = 5.5–7.5. However, initial pH has a negative cumulative effect on the adsorption. Interaction affects of both initial pH and temperature with initial concentration were considered as significant parameters on the adsorption process.

The optimum points giving the maximum uptake of uranium ions (435 mg g^{-1}) were found to be at initial pH of 4.2, temperature of 60 °C, initial concentration of 90 mg L^{-1} and shaking time of 173 min.

In order to identify the adsorption process, adsorption data were fitted by isotherm models and thermodynamic parameters were calculated. The results showed that the adsorption of uranium on NH_2–MCM-41 was described as an isotherm of Langmuir monolayer type, ion exchange mechanism, endothermic, spontaneous and favorable.

It can be concluded that NH_2–MCM-41 may be used as an efficient adsorbent for UO_2^{2+} uptake from aqueous solutions. The experimental studies showed that NH_2–MCM-41 can be used for preventing environmental contamination and for the removal of uranium from wastes in various stages of nuclear fuel production depending on the uranium fuel cycle.

Acknowledgement

The authors thank the Ege University Scientific Research Fund for financial support (Project No. 2007 NBE 001).

References

[1] A. Krestou, A. Xenidis, D. Panias, Miner. Eng. 17 (2004) 373–381.
[2] T.S. Anirudhan, P.G. Radhakrishnan, J. Environ. Radioact. 100 (2009) 250–257.
[3] S.V. Bhat, J.S. Meloa, B.B. Chaugule, S.F. D'Souza, J. Hazard. Mater. 158 (2008) 628–635.
[4] M. Saleem, M. Afzal, R. Qadeer, J. Hanif, Selective adsorption of uranium on activated charcoal from electrolytic aqueous solutions, Sep. Sci. Technol. 27 (1992) 239.
[5] C. Kütahyalı, M. Eral, Sep. Purif. Technol. 40 (2004) 109–114.
[6] S. Aytas, S. Akyıl, M. Eral, J. Radioanal. Nucl. Chem. 260 (1) (2004) 119–125.
[7] T.E. Paynea, J.A. Davis, G.R. Lumpkina, R. Chisaria, T.D. Waite, Appl. Clay Sci. (2004) 26151–26162.
[8] S. Aytas, M. Yurtlu, R. Donat, J. Hazard. Mater. 172 (2009) (2009) 667–674.
[9] C.J.C. Brause, J.M. Berg, R.A. Matzner, D.E. Morris, J. Colloid Interface Sci. 233 (2001) 38–49.
[10] C. Gok, S. Aytas, J. Hazard. Mater. 168 (2009) 369–375.
[11] T. Missana, M.G. Gutiérrez, Colloid Interface Sci. 260 (2003) 291–301.
[12] S. Yusan, S. Akyıl, J. Hazard. Mater. 160 (2008) 388–395.
[13] J.S. Beck, J.C. Vartuli, W.J. Roth, M.E. Leonowicz, C.T. Kresge, K.D. Schmitt', C.T.W. Chu, D.H. Olson, E.W. Sheppard, S.B. McCullen, J.B. Higgins, J.L. Schlenkert, J. Am. Chem. Sot. 114 (1992) 10834–10843.
[14] C.T. Kresge, M.E. Leonowicz, W.C. Roth, J.C. Vartuli, J.S. Beck, Lett. Nat. 359 (1992) 710–712.
[15] A.S. Araujo, V.J. Fernandes Jr., S.A. Verissimo, J. Therm. Anal. Calorim. 59 (2000) 649–655.
[16] A. Taguchi, F. Schuth, Microporous Mesoporous Mater. 77 (2005) 1–45.
[17] K. Stamberg, K.A. Venkatesan, P.R. Vasudeva Rao, Colloids Surf. A. 221 (2003) 149/162.
[18] M.R. Jamali, Y. Assadi, F. Shemirani, M.R.M. Hosseini, R.R. Kozani, M.M. Farahani, M.S. Niasari, Anal. Chim. Acta 579 (2006) 68–73.
[19] K.P. Lee, A.M. Showkat, A.I. Gopalan, IAEA-TECDOC-1465 (2005) 109–120.
[20] G.E. Fryxell, Y. Lin, S. Fiskum, J.C. Birnbaum, H. Wu, Environ. Sci. Technol. 39 (2005) 1324–1331.
[21] J.C. Birnbaum, B. Busche, Y. Lin, W.J. Shaw, G.E. Fryxell, Chem. Commun. (2002) 1374–1375.
[22] G.E. Fryxell, H. Wu, Y. Lin, J.W. Shaw, J.C. Birnbaum, J.C. Linehan, Z. Nie, K. Kemner, S.J. Kelly, Mater. Chem. 14 (2004) 3356–3363.
[23] K.F. Lam, K.L. Yeung, G. Mckay, Microporous Mesoporous Mater. 100 (2007) 191–201.
[24] D.P. Quintanilla, I. Hierro, M. Fajardo, I. Sierra, J. Environ. Monit. 8 (2006) 214–222.
[25] T. Yokoi, T. Tatsumi, H. Yoshitake, J. Colloid Interface Sci. 274 (2004) 451–457.
[26] L. Mercier, T.J. Pinnavaia, Environ. Sci. Technol. 32 (1998) 2749–2754.
[27] I. Rafiqul, B. Lugang, Y. Yan, T. Li, Fuel Process. Technol. 68 (1) (2000) 3–12.
[28] Q. Cai, W.Y. Lin, F.S. Xiao, W.Q. Pang, X.H. Chen, B.S. Zou, Microporous Mesoporous Mater. 32 (1999) 1–15.
[29] M.E. Mahmoud, I.M.M. Kenawy, E.M. Soliman, M.A. Hafez, M.A.A. Akl, E.E.A. Lashein, Anal. Sci. 24 (March) (2008).
[30] Y. Shiraishi, G. Nishimura, T. Hirai, I. Komasawa, Ind. Eng. Chem. Res. 41 (2002) 5065–5070.
[31] A. Heidari, H. Younesi, Z. Mehraban, Chem. Eng. J. 153 (2009) 70–79.
[32] M. Manzano, V. Aina, C.O. Aréan, F. Balas, V. Cauda, M. Colilla, M.R. Delgado, M. Vallet-Reǵ, Chem. Eng. J. 137 (2008) 30–37.
[33] D.C. Montgomery, Design and Analysis of Experiments, fourth ed., John Wiley &Sons, USA, 1996.
[34] M.A. Bezerra, R.E. Santelli, P.E. Oliveira, L.S. Villar, L.A. Escaleira, Talanta 76 (2008) 965–977.
[35] M.Y. Cana, E. Yıldız, J. Hazard. Mater. B135 (2006) 165–170.
[36] M.E.R. Carmona, M.A.P. da Silva, S.G.F. Leite, Process Biochem. 40 (2005) 779–788.
[37] S.V. Bhat, J.S. Meloa, B.B. Chaugule, S.F. D'Souza, Biosorption characteristics of uranium(VI) from aqueous medium onto *Catenella repens*, a red alga, J. Hazard. Mater. 158 (2008) 628–635.
[38] F. Ghorbania, H. Younesia, S.M. Ghasempouria, A.A. Zinatizadeh, M. Aminia, A. Daneshia, Chem. Eng. J. 145 (2008) 267–275.
[39] R. Han, W. Zou, Y. Wang, L. Zhu, J. Environ. Radioact. 93 (2007) 127–143.
[40] A.M. Donia, A.A. Atia, E. M.M. Moussa, A.M. El-Sherif, M.O.A. El-Magied, Hydrometallurgy 95 (2000) 183–189.
[41] C. Kütahyalı, M. Eral, J. Nucl. Mater. 396 (2010) 251–256.
[42] N. Ünlü, M. Ersoz, J. Hazard. Mater. B136 (2006) 272–280.